Articles

Contribution from the Department of Chemistry, Willard H. Dow Laboratories, University of Michigan, Ann Arbor, Michigan 48109-1055

Manganese Complexes of α-Hydroxy Acids

Salman M. Saadeh, Myoung Soo Lah, and Vincent L. Pecoraro*

Received June 19, 1990

Manganese complexes of α-hydroxy acids (H_2L) have been implicated in the basidomycete oxidative degradation pathway of lignin. In this contribution, we evaluate the chemistry of manganese(III) and manganese(IV) α-hydroxy acid compounds using lactic acid (H_2Lc), 2-hydroxy-2-ethylbutyric acid (H_2HEB), and 2-hydroxyisobutyric acid (H_2HIB). Both oxidative and reductive methodologies to give compounds of stoichiometry $(Cat)_3[(Cat)Mn^{IV}_2L_6]$, $(Cat)_3[Mn^{III}_2(L)_4HL]$ and $(Cat)_2[Mn^{III}(L)_2HL]$ have been explored. The X-ray structure of **1**, $Na_3[NaMn^{IV}_2(HIB)_6]\cdot 4MeOH$, which was prepared by the reaction of $MnCl_2$, H_2HIB, and $NaOCH_3$ in methanol, reveals a mixed-metal trinuclear cluster composed of two Mn(IV) octahedra that are bridged by a sodium ion. The face-shared geometry leads to a very short Mn–Na distance (2.98 Å). **1** is a unique Mn(IV) complex with all oxygen ligation and containing redox-innocent ligands. The O(3)O(3′) coordination shell is trigonally compressed along the face containing the three alkoxide ligands. The X-band EPR spectrum of **1** at 100 K is consistent with an isolated $S = {}^3/_2$ spin system. The Mn(III) dimer $(TMA)_3[Mn^{III}_2(Lc)_4HLc]\cdot H_2O$ (**5**) can be prepared by the reaction of tetramethylammonium permanganate ($(TMA)MnO_4$), H_2Lc, and (TMA)OH in methanol. An excess of ligand allows for the reduction of the Mn(VII) to Mn(III). The X-ray structure of **5** provides the first example of an Mn(III) dimer with axial compression. Two $Mn^{III}Lc_2$ units, having a propeller configuration, are bridged by the carboxylate of an HLc^-, having a protonated hydroxyl oxygen atom, and weak bridges from coordinated alkoxides of the adjacent $Mn^{III}Lc_2$ unit. The Mn–Mn separation is 3.09 Å. A third compound of composition $(Cat)_2[Mn^{III}(L)_2HL]$ has also been prepared by both reductive and oxidative methodologies and is most likely an infinite chain structure that has a *trans*-$Mn^{III}L_2$ plane that is linked by the anti–anti coordination of carboxylate oxygens of an HL^-. The relevance of these manganese α-hydroxy acid complexes to structural proposals for the oxygen-evolving complex and diffusible intermediates of the manganese lignin peroxidase is discussed. X-ray parameters for $Na_3[NaMn^{IV}_2(HIB)_6]\cdot 4MeOH$ (**1**) $Na_4Mn_2C_{28}H_{52}O_{22}$: 942.6 g/mol, triclinic crystal system, $P\bar{1}$, $a = 9.549$ (6) Å, $b = 9.843$ (4) Å, $c = 13.966$ (8) Å, $\alpha = 108.12$ (4)°, $\beta = 76.44$ (5)°, $\gamma = 119.61$ (4)°, $V = 1079$ (1) Å^3, $Z = 1$, 2845 data collected with $3° < 2\theta < 45°$, 2216 data with $I > 3\sigma(I)$, $R = 0.057$, $R_w = 0.058$. X-ray parameters for $(TMA)_3[Mn^{III}_2(Lc)_4HLc]\cdot H_2O$ (**5**), $Mn_2C_{27}H_{59}N_3O_{16}$: 791 g/mol, monoclinic crystal system, $P2_1$, $a = 11.425$ (6) Å, $b = 15.214$ (10) Å, $c = 12.108$ (4) Å, $\beta = 106.45$ (3)°, $V = 2018$ (2) Å^3, $Z = 2$, 2767 data collected with $3° < 2\theta < 45°$, 1719 data with $I > 3\sigma(I)$, $R = 0.057$, $R_w = 0.058$.

Introduction

Inorganic chemists have focused much attention on a structural description of the metallocenter(s) of manganese requiring enzymes over the past 10 years.[1-5] Chief among the systems of interest is the oxygen-evolving complex[6] (OEC) that converts two molecules of water to dioxygen, four protons, and four electrons (eq 1). There are three basic proposals for the organization of

$$2H_2O \rightarrow O_2 + 4H^+ + 4e^- \quad (1)$$

manganese ions in this enzyme: (A) a single, tetranuclear clus-

(1) (a) Li, X.; Pecoraro, V. L. *Inorg. Chem.* **1989**, *28*, 3403. (b) Pecoraro, V. L. In *Manganese Redox Enzymes*; Pecoraro, V. L., Ed.; Verlag-Chemie: New York, in press; Chapter 13. (c) Li, X.; Lah, M. S.; Pecoraro, V. L. *Acta Crystallogr. Sect.* **1989**, *C45*, 1517. (d) Bonadies, J. A.; Kirk, M. L.; Kessissoglou, D. P.; Lah, M. S.; Hatfield, W. E.; Pecoraro, V. L. *Inorg. Chem.* **1989**, *28*, 2037. (e) Bonadies, J. A.; Maroney, M. J.; Pecoraro, V. L. *Inorg. Chem.* **1989**, *28*, 2044. (f) Kessissoglou, D. P.; Bender, C.; Kirk, M. L.; Lah, M. S.; Pecoraro, V. L. *J. Chem. Soc., Chem. Commun.* **1989**, 84. (g) Kessissoglou, D. P.; Li, X.; Kirk, M.; Pecoraro, V. L. *Inorg. Chem.* **1988**, *27*, 1. (h) Kessissoglou, D. P.; Li, X.; Butler, W. M.; Pecoraro, V. L. *Inorg. Chem.* **1987**, *26*, 2487. (i) Pecoraro, V. L.; Li, X.; Baker, M. J.; Butler, W. M.; Bonadies, J. A. *Rec. Trav. Chim. Pays-Bas* **1987**, *106*, 221. (j) Kessissoglou, D. P.; Butler, W. M.; Pecoraro, V. L. *Inorg. Chem.* **1987**, *26*, 495. (k) Pecoraro, V. L.; Kessissoglou, D. P.; Li, X.; Butler, W. M. *Prog. Photosynth. Res.* **1987**, *1*, 795. (l) Kessissoglou, D. P.; Butler, W. M.; Pecoraro, V. L. *J. Chem. Soc., Chem. Commun.* **1986**, 1253. (m) Pecoraro, V. L.; Butler, W. M. *Acta Crystallogr., Sect. C* **1986**, *C42*, 1151. (n) Lah, M. S.; Pecoraro, V. L. *J. Am. Chem. Soc.* **1989**, *111*, 7258. (o) Pecoraro, V. L.; Kessissoglou, D. P.; Li, X.; Lah, M. S.; Saadeh, S.; Bender, C.; Bonadies, J. A.; Larson, E. *Prog. Photosynth. Res.* **1990**, *1*, 770.

(2) Vincent, J. B.; Christmas, C.; Huffman, J. C.; Christou, G.; Chang, H.-R.; Hendrickson, *J. Chem. Soc., Chem. Commun.* **1987**, 236; Christmas, C.; Vincent, J. B.; Huffman, J. C.; Christou, G.; Chang, H.-R.; Hendrickson, D. N. *J. Chem. Soc., Chem. Commun.* **1987**, 1303. Bashkin, J. S.; Chang, H.-R.; Streib, W. E.; Huffman, J. C.; Hendrickson, D. N.; Christou, G. *J. Am. Chem. Soc.* **1987**, *109*, 6502. Vincent, J. B.; Christou, G. *Adv. Inorg. Chem.* **1989**, *33*, 197.

(3) (a) Kipke, C. A.; Scott, M. J.; Goehdes, J. W.; Armstrong, W. A. *Inorg. Chem.* **1990**, *29*, 2193. (b) Chan, M. K.; Armstrong, W. A. *J. Am. Chem. Soc.* **1989**, *111*, 9121.

(4) (a) Wieghardt, K.; Bossek, U.; Bonvoisin, J.; Beauvillain, P.; Girerd, J.-J.; Nuber, B.; Weiss, J.; Heinze, H. *Angew. Chem., Int. Ed. Engl.* **1986**, *25*, 1030. (b) Wieghardt, K.; Bossek, U.; Zsolnai, L.; Huttner, G.; Blondin, G.; Girerd, J.-J.; Babonneau, F. *J. Chem. Soc., Chem. Commun.* **1987**, 651. (c) Wieghardt, K.; Bossek, U.; Nuber, B.; Weiss, J.; Bonvoisin, J.; Corbella, M.; Vitols, S. E.; Girerd, J.-J. *J. Am. Chem. Soc.* **1988**, *110*, 7398. (d) Wieghardt, K.; Bossek, U.; Ventur, D.; Weiss, J. *J. Chem. Soc., Chem. Commun.* **1985**, 347. (e) Wieghardt, K.; Bossek, U.; Gebert, W. *Angew. Chem., Int. Ed. Engl.* **1983**, *22*, 328.

(5) (a) Sheets, J. E.; Czernuszewicz, R. S.; Dismukes, G. C.; Rheingold, A. L.; Petroleas, V.; Stubbe, J.; Armstrong, W. H.; Beer, R. H.; Lippard, S. J. *J. Am. Chem. Soc.* **1987**, *109*, 1435. (b) Nishida, Y.; Oshino, N.; Tokii, T. *Z. Naturforsch.* **1988**, *43B*, 472. (c) Mikuriya, M.; Torihara, N.; Okawa, H.; Kida, S. *Bull. Chem. Soc. Jpn.* **1981**, *54*, 1063. (d) McKee, V.; Shepard, W. B. *J. Chem. Soc., Chem. Commun.* **1985**, 158. (e) Brooker, S.; McKee, V.; Shepard, W. B.; Pannell, L. *J. Chem. Soc, Dalton Trans.* **1987**, 2555. (f) Mabad, B.; Tuchages, J.-P.; Hwang, Y. T.; Hendrickson, D. N. *J. Am. Chem. Soc.* **1985**, *107*, 2801. (g) Bhula, R.; Gainsford, G. J.; Weatherburn, D. C. *J. Am. Chem. Soc.* **1988**, *110*, 7550. (h) Diril, H.; Chang, H. R.; Zhang, X.; Potenza, J. A.; Shugar, H. A.; Hendrickson, D. N.; Isied, S. S. *J. Am. Chem. Soc.* **1987**, *109*, 6207.

(6) Recent reviews of this subject include: (a) Pecoraro, V. L. *Photochem. Photobiol.* **1988**, *48*, 249. (b) Babcock, G. T. *Comprehensive Biochemistry: Photosynthesis*; Amesz, J., Ed.; Elsevier-North Holland: Amsterdam, 1987, Vol. 15, p 121. (c) Asmez, J. *Biochim. Biophys. Acta* **1983**, *726*, 1. (d) Ghanotakis, D.; Yocum, C. F. *Annu. Rev. Plant Physiol. Mol. Biol.* **1990**, *41*, 255. (e) Christou, G. *Accts. Chem. Res.* **1989**, *22*, 328. (f) Wieghardt, K. *Angew. Chem. Int. Ed. Engl.* **1990**, *28*, 1153. (g) Rutherford, A. W. *Trends Biochem. Sci.* **1989**, *14*, 227. (h) Larson, E.; Pecoraro, V. L. In *Manganese Redox Enzymes*; Pecoraro, V. L., Ed.; Verlag-Chemie: New York, in press; Chapter 1.

0020-1669/91/1330-0008$02.50/0

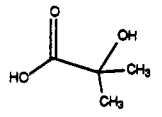

H_2HIB

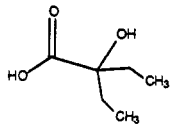

H_2HEB

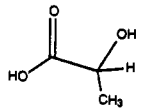

H_2Lc

Figure 1. Ligands used in this study: 2-hydroxyisobutyric acid (H_2HIB); 2-hydroxy-2-ethylbutyric acid (H_2HEB); lactic acid (H_2Lc).

ter,[2,7,8] (B) mononuclear and trinuclear centers,[1,9] or (C) two dimers.[10] Hannson et al.[11] assigned the low-field EPR signal ($g \approx 4.1$) in the S_2 state of the OEC to a mononuclear Mn(IV) with unknown protein ligands. This suggestion formed the basis for a dual center model, which eventually developed into proposal B above. Unfortunately, structurally characterized mononuclear Mn(IV) compounds containing exclusively biologically relevant heteroatom donors with reported EPR spectra are rare. To evaluate this proposal critically, one must catalogue spectra of manganese(IV) in a variety of coordination modes and with different ligand sets. Examples of N_2O_4 complexes are available[1c,h,12] that span a wide range of redox potentials. Previous reports of mononuclear manganese(IV) coordination compounds with an O_6 donor environment are limited to the [tris(3,5-di-*tert*-butylpyrocatecholato)manganate(IV)]$^{2-}$ anion {$Mn(DTBC)_3^{2-}$} as the potassium[13] and sodium[14] salts and bis(triethylammonium) tris(pyrocatecholato)manganate(IV).[13b] Although quinones are important components of the photosystem reaction center, it appears that the redox-noninnocent series of ligands (quinone, semiquinone, and hydroquinone) are not bound to the manganese atoms in the OEC.[15] Therefore, we perceived a need to characterize $Mn^{IV}O_6$ complexes with carboxylate and alkoxide ligands that better mimic probable active site residues.

Table I. Physical Parameters of Manganese α-Hydroxy Acid Complexes

complex	UV-vis λ, nm (ε)	EPR[a]	μ_{eff}, μ_B
1	550 (414)	4.25,[b] 1.98 (84)[b]	3.98 (methanol)
		5.96 (71)[c]	4.01 (solid)
2		4.25,[b] 1.98[b] (100)[d]	*d*
		5.96 (75)[c]	
5	410 (730)	silent	6.8 (solid)[e]
6	405 (296)	silent	4.94 (acetonitrile)
	515 (140)		4.71 (solid)

[a] g_{eff} values. ^{55}Mn hyperfine coupling, when observed, is reported in parentheses in gauss. [b] Major component. [c] Minor component. [d] This compound was always isolated with a small degree of Mn(II) impurity. Therefore, we were unable to obtain reliable magnetic data. [e] This corresponds to 4.8 μ_B/Mn.

In addition to the OEC, other manganese-requiring enzymes include manganese catalases[16-18] that disproportionate hydrogen peroxide to dioxygen and water (eq 2) and manganese superoxide

$$2H_2O_2 \rightarrow O_2 + 2H_2O \quad (2)$$

$$2HO_2 \rightarrow O_2 + H_2O_2 \quad (3)$$

dismutases[19] that convert hydrogen superoxide to dioxygen and hydrogen peroxide (eq 3). One enzyme that has received relatively little attention is the manganese peroxidase[20] from the basidomycete *Phanerochaete chrysosporium*, which is thought to use a diffusible manganese α-hydroxy acid complex to decompose lignin. It was reasonably proposed that α-hydroxy acids might stabilize the Mn(III) oxidation level; however, there is little experimental literature based on structurally well-defined, chemically characterized manganese complexes of α-hydroxy acids to evaluate this idea.

An understanding of the chemistry of manganese α-hydroxy acid complexes would provide valuable information about two of the enzymes described above. In a direct way, one could evaluate the stable oxidation levels, available structural types, and reactivity properties of compounds that are proposed intermediates of the lignin degradation reaction. In an indirect way, these compounds can be used to evaluate nuclearity proposals for the OEC.

We reasoned that α-hydroxy acids (Figure 1), which previously were shown[21] to form high valent metal complexes such as $[Cr^VO(L)_2]^-$, would provide the characteristics required to generate high-oxidation-state manganese complexes with biologically relevant, redox-inert ligands. Our synthetic strategy included both oxidative and reductive approaches, which led to complexes of the stoichiometry $Mn^{IV}L_3^{2-}$, $Mn^{III}L_2HL^{2-}$, and $Mn^{III}{}_2L_4HL^{3-}$ depending on the steric bulk of the ligands employed. Herein, we provide the structural characterization of sterically unhindered complexes that are the first discrete mononuclear Mn(IV) compounds containing an all oxygen, redox-innocent set of donor atoms and specifically compare the spectroscopic properties to the $g =$

(7) (a) Brudvig, G. W.; Crabtree, R. *Proc. Natl. Acad. Sci. U.S.A.* **1986**, *83*, 4586. (b) Brudvig, G. W. *ACS Symp. Ser.* **1988**, *372*, 221. (c) dePaula, J. C.; Beck, W. F.; Brudvig, G. W. *J. Am. Chem. Soc.* **1986**, *108*, 4002.
(8) Dismukes, G. C. *Photochem. Photobiol.* **1986**, *43*, 99.
(9) Penner-Hahn, J. E.; Fronko, R.; Pecoraro, V. L.; Bowlby, N. F.; Betts, S. D.; Yocum, C. F. *J. Am. Chem. Soc.* **1990**, *112*, 2549.
(10) Guiles, R. D.; McDermott, A.; Yachandra, V. K.; Cole, J. L.; Dexheimer, S. L.; Britt, R. D.; Wieghardt, K.; Bossek, U.; Sauer, K.; Klein, M. P. *Biochemistry* **1990**, *29*, 471. Guiles, R. D.; Yachandra, V. K.; McDermott, A.; Cole, J. L.; Dexheimer, S. L.; Britt, R. D.; Sauer, K.; Klein, M. P. *Biochemistry* **1990**, *29*, 486. Yachandra, V. K.; Guiles, R. D.; McDermott, A.; Britt, R. D.; Dexheimer, S. L.; Sauer, K.; Klein, M. P. *Biochim. Biophys. Acta* **1986**, *850*, 324. Yachandra, V. K.; Guiles, R. D.; McDermott, A.; Cole, J. L.; Britt, R. D.; Dexheimer, S. L.; Sauer, K.; Klein, M. P. *Biochemistry* **1987**, *26*, 5974. Kirby, J. A.; Goodin, D. B.; Wydrzynski, T.; Robertson, A. S.; Klein, M. P. *J. Am. Chem. Soc.* **1981**, *103*, 5529. Kirby, J. A.; Robertson, A. S.; Smith, J. P.; Thompson, A. C.; Cooper, S. R.; Klein, M. P. *J. Am. Chem. Soc.* **1981**, *103*, 5537.
(11) Hansson, O. R.; Aasa, R.; Vänngard, T. *Biophys. J.* **1987**, *51*, 825.
(12) Pavacik, P. S.; Huffman, J. C.; Christou, G. *J. Chem. Soc., Chem. Commun.* **1986**, 43.
(13) (a) Hartman, J. A.; Foxman, B. M.; Cooper, S. R. *J. Chem. Soc., Chem. Commun.* **1982**, 583. (b) Hartman, J. A.; Foxman, B. M.; Cooper, S. R. *Inorg. Chem.* **1984**, *23*, 1381.
(14) Chin, D.-H.; Sawyer, D. T.; Schaefer, W. P.; Simmons, C. J. *Inorg. Chem.* **1983**, *22*, 752.
(15) Ohno, T.; Satoh, K.; Katoh, S. *Biochim. Biophys. Acta* **1986**, *852*, 1.
(16) Barynin, V. V.; Vagin, A. A.; Melik-Adamyin, V. R.; Grebenko, A. I.; Khangulov, S. V.; Popov, A. N.; Anrianova, M. E.; Vainshtein, B. K. *Sov. Phys.—Dokl. (Engl. Transl.)* **1986**, *31*, 457. Khangulov, S. V.; Barynin, V. V.; Melik-Adamyin, V. R.; Grebenko, A. I.; Voevodskaya, N. V.; Blumenfeld, L. A.; Dobryakov, S. N.; Il'Yasova, V. B. *Bioorg. Khim.* **1986**, *12*, 741.
(17) Fronko, R.; Penner-Hahn, J. E.; Bender, C. *J. Am. Chem. Soc.* **1988**, *110*, 7554. Penner-Hahn, J. E. In *Manganese Redox Enzymes*; Pecoraro, V. L., Ed.; Verlag-Chemie: New York, in press; Chapter 2.
(18) Kono, Y.; Fridovich, I. *J. Biol. Chem.* **1983**, *258*, 13646. Beyer, W. F., Jr.; Fridovich, I. *Biochemistry* **1985**, *24*, 6460.
(19) Ludwig, M. L.; Pattridge, K. A.; Stallings, W. C. *Metabolism and Enzyme Function*; Academic Press, Inc.: New York, 1986; p 405. Stallings, W. C.; Pattridge, K. A.; Strong, R. K.; Ludwig, M. L. *J. Biol. Chem.* **1985**, *260*, 16424.
(20) Wariishi, H.; Akileswaran, L.; Gold, M. H. *Biochemistry* **1988**, *27*, 5365. Glenn, J. K.; Akileswaran, L.; Gold, M. H. *Arch. Biochem. Biophys.* **1986**, *251*, 688.
(21) Krumpolc, M.; Rocek, J. *J. Am. Chem. Soc.* **1979**, *101*, 3206.

4 signal of the S_2 state of the OEC. Furthermore, we report the first example of an axially compressed Mn(III) dimer. We also illustrate that as bulky substituents are added to the ligands, the Mn(III) oxidation level is stabilized.

Experimental Section

Materials and Methods. Abbreviations used: H_2HIB = 2-Hydroxyisobutyric acid; H_2Lc = lactic acid; H_2HEB = 2-hydroxy-2-butyric acid; TBA = tetra-*n*-butyl ammonium; TMA = tetramethyl ammonium. H_2HIB, H_2HEB, H_2Lc, $KMnO_4$, and $NaMnO_4$ were purchased from Aldrich Chemical Co. Tetra-*n*-butyl ammonium or tetramethyl ammonium permanganates [(TBA)MnO_4, (TMA)MnO_4] were prepared by a metathesis reaction of the alkylammonium chloride and $KMnO_4$. Tetra-*n*-butyl ammonium hexafluorophosphate [(TBA)PF_6] was made by the metathesis of tetra-*n*-butyl ammonium bromide and ammonium hexafluorophosphate in water and recrystallized from hot ethanol prior to electrochemical studies. High-purity solvents for electrochemical studies were purchased from American Burdick and Jackson Co. and used as received. These solvents were stored under nitrogen. High-purity argon gas was used to deaerate solutions. All other chemicals and solvents were reagent grade. Chemical analyses were performed in the Chemical Analysis Laboratory in the Chemistry Department at the University of Michigan.

Synthesis of Complexes. Preparation of Mn(IV) Complexes. The synthetic procedure for the preparation of $[Mn^{IV}L_3]^{2-}$, where L = 2-hydroxyisobutyric acid, can be achieved via oxidative or reductive approaches. For the highest yields, it is very important to carefully dry all solvents, as the Mn(IV) materials are moderately water-sensitive. The physical properties of the complexes are provided in Table I. Analyses for all salts of the complexes are equally consistent with the presented formulations. Thus, unless otherwise indicated, analyses are provided only for the sodium salts. The $[Mn^{IV}(Lc)_3]^{2-}$ ion could be detected only by using the oxidative procedure.

(Cat)$_2$[Mn(HIB)$_3$]·2CH$_3$OH (Where Cat = Na (1), K (2), TMA (3)). Oxidative Procedure Using Mn(II) Salts. A colorless solution is obtained when 2 equiv of 2-hydroxyisobutyric acid is reacted with 1 equiv of $MnCl_2·4H_2O$ in methanol. A reddish pink solution is then generated after 6 equiv of sodium methoxide is slowly added to this solution. The oxidant in these cases is atmospheric oxygen. If the base is added too rapidly, a white precipitate containing Mn(II) is formed. Deep red crystals of $Na_2[Mn(HIB)_3]·2CH_3OH$ (**1**) were obtained upon slow evaporation after filtration of the reaction mixture. These crystals were used in the X-ray analysis. The $(TMA)_2[Mn(Lc)_3]·2CH_3OH$ (**4**) could be detected in situ; however, it decomposed rapidly to a manganese(III) lactate complex described below. Anal. Calcd for **1**, $Na_2[Mn(HIB)_3]·2CH_3OH$ ($Na_2Mn_1C_{14}H_{26}O_{11}$, MW = 471.2): Na, 9.76; Mn, 11.67; C, 35.65; H, 5.52. Found: Na, 10.17; Mn, 11.75; C, 34.25; H, 5.12.

Reductive Procedure Using Salts of Permanganate. *Caution! Alkylammonium permanganates are highly explosive!! Do not dry any such permanganate salts!* A 30-mL degassed methanol solution of 1.04 g of H_2HIB (0.010 mol) was transfered by cannula to 10 mL of a deep violet acetone solution of 0.312 g of sodium permanganate (0.0022 mole). After the evolution of CO_2, the resulting mixture was reddish brown. Base, in the form of 0.088 g of NaOH (0.0022 mol), was added to neutralize this solution. A deep red solid can be isolated by the slow addition of hexane or diethyl ether. Compounds with identical complex stoichiometry are obtained as potassium (**2**) and tetra-*n*-methylammonium (**3**) salts when $KMnO_4$ and (TMA)MnO_4 are metal sources. Anal. Calcd for **2**, $K_2[Mn(HIB)_3]·2H_2O$ ($K_2MnC_{12}H_{22}O_{11}$, MW = 475): K, 16.45; Mn, 11.56; C, 30.31; H, 4.66. Found: K, 16.96; Mn, 11.46; C, 30.56; H, 4.46.

Preparation of Mn(III) Complexes. The preparation of $[Mn^{III}L_3]^{2-}$ where L = 2-hydroxy-2-ethylbutyric and lactic acids with the use of reductive methodologies is described below for the HEB complexes. Using different conditions a lactate-bridged dimer ($(TMA)_3[Mn_2(Lc)_5]$) may also be isolated from the reductive procedure. The oxidative approach did not lead to pure complexes. Physical properties of each complex are given in Table I.

(TMA)$_3$[Mn$_2$(Lc)$_2$HLc] (5). Reductive Procedure Using Tetramethylammonium Permanganate. *Caution! Alkylammonium permanganates are highly explosive!! Do not dry any such permanganate salts!* A deep violet acetone solution of tetramethyl ammonium permanganate (15 mL, 0.003 mol) was added to a 30-mL acetone solution of H_2Lc (0.011 mol) and tetramethylammonium hydroxide (0.003 mol) and the mixture stirred for 5 h at which point a dark precipitate had deposited. The acetone was decanted and the solid washed with acetone/diethyl ether. The solid was redissolved in methanol, filtered, flash evaporated, and then redissolved in ethanol. X-ray quality crystals were deposited after a few days by diffusion with pentane. This material is slightly hygroscopic. Anal. Calcd for **5**, $(TMA)_3[Mn_2(Lc)_4HLc]·H_2O$ ($Mn_2C_{27}H_{59}N_3O_{16}$): Mn, 13.60; C, 40.05; H, 7.54; N, 5.19. Found: Mn, 13.13; C, 39.94; H, 7.06; N, 5.27.

Table II. Crystallographic Parameters for $Na_3[NaMn^{IV}_2(HIB)_6]·4MeOH$ (**1**) and $(TMA)_3[Mn^{III}_2(Lc)_4HLc]·H_2O$ (**5**)

formula	$Na_4Mn_2C_{28}H_{52}O_{22}$	$Mn_2C_{27}H_{59}N_3O_{16}$
mol wt	942.6	791
a, Å	9.549 (6)	11.425 (6)
b, Å	9.843 (4)	15.214 (10)
c, Å	13.966 (8)	12.108 (4)
α, deg	108.12 (4)	
β, deg	76.44 (5)	106.45 (3)
γ, deg	119.61 (4)	
V, Å^3	1079 (1)	2018 (2)
cryst syst	triclinic	monoclinic
space group	$P\bar{1}$	$P2_1$
d_{calc}, g/mL	1.450	1.303
d_{obs}, g/mL	1.44	1.33
Z	1	2
radiation	Mo Kα (0.7107 Å)	Mo Kα (0.7107 Å)
abs coeff (μ), cm^{-1}	6.45	6.6
temp, K	298	298
cryst size, mm	0.17 × 0.32 × 0.27	0.14 × 0.20 × 0.30
scan speed, deg/min	2.5–12	2.5–12
scan range, deg	$3 < 2\theta < 45$	$3 < 2\theta < 45$
bkdg/scan time ratio	0.8	0.8
no. of unique data collcd	2845	2767
no. of obsd data ($I > 3\sigma(I)$)	2216	1719
largest residual	0.68	0.62
R	0.057	0.057
R_w	0.058	0.058

{(TBA)$_2$[Mn(HEB)$_2$HHEB]}$_n$ (6) and {(Na)$_2$[Mn(Lc)$_2$HLc]·H$_2$O}$_n$ (7). *Caution! Alkylammonium permanganates are highly explosive!! Do not dry any such permanganate salts!* A 30-mL acetone solution of H_2HEB (0.03 mol) was added to 10 mL of a deep violet acetone solution of tetra-*n*-butyl ammonium permanganate (0.01 mol). After the evolution of CO_2, the resulting solution was flash evaporated and the residue dried under vacuum. Crystals of **6** were obtained by slow evaporation or hexane diffusion into a THF solution. A similar Mn(III)-containing material was isolated when permanganate salts were reacted with lactic acid and the corresponding base using a 2:7.5:2 ratio. In this case, elemental analysis and infrared spectra are consistent with the formula unit $Na_2[Mn(Lc)_2HLc]$ (**7**). Anal. Calcd for **6**, $(TBA)_2[Mn(HEB)_2HHEB]$ ($MnC_{50}H_{102}N_2O_9$): Mn, 5.92; C, 64.58; H, 10.98; N, 3.01. Found: Mn, 5.52; C, 64.56; H, 11.24; N, 3.04. Anal. Calcd for **7**, $Na_2[Mn(Lc)_2HLc]·H_2O$ ($Na_2Mn_1C_9H_{15}O_{10}$): Na, 12,01; Mn, 14.32; C, 28.12; H, 3.94. Found: Na, 11.84; Mn, 14.42; C, 28.47; H, 4.10.

Methods. Infrared spectra were obtained on a Nicolet 60-SX FT-IR as KBr pellets. Room-temperature solid-state magnetic moments were calculated from data obtained on a Johnson-Mathey magnetic susceptibility balance. Solution susceptibilities were calculated from data obtained with a Bruker 360-MHz NMR spectrometer by using the Evans method.[22] Solution EPR spectra were recorded on a Bruker ER200 E-SRC spectrometer equipped with a liquid-nitrogen Dewar and a Varian variable-temperature controller. DPPH (g = 2.0037) was used as an external standard. Electrochemical measurements were completed at 23 ± 2 °C on a BAS-100 electrochemical analyzer. Cyclic voltammetry was performed by using a three-electrode system composed of platinum-bead, platinum-wire, and saturated calomel (SCE, within a Lugin probe) electrodes as the working, auxiliary, and reference electrodes, respectively. (TBA)PF_6 was used as the supporting electrolyte at 0.1 M concentration. All potentials are referenced versus the ferrocene/ferrocenium couple employed as an external reference. UV/vis spectra were recorded on a Perkin-Elmer Lambda 9 UV/vis near-IR spectrophotometer equipped with a Perkin-Elmer 3600 data station.

Collection and Reduction of X-ray Data. Single crystals of **1** were grown from methanol, and **5** was isolated by vapor diffusion of pentane into an ethanol solution of **5**. Each crystal was then mounted in a glass capillary, and data were collected on a Syntex $P2_1$ diffractometer. Intensity data were obtained by using Mo Kα radiation (0.7107 Å) monochromatized from a graphite crystal whose diffraction vector was parallel to the diffraction vector of the sample. Three standard reflections were measured every 50 reflections. Lattice parameters were determined

(22) Evans, D. F. *J. Chem. Soc.* **1959**, 2003. Bartle, K. D.; Dale, B. J.; Jones, D. W.; Maricic, J. *J. Magn. Reson.* **1973**, *12*, 286.

Table III. Fractional Atomic Coordinates for $Na_3[NaMn^{IV}_2(HIB)_6]\cdot 4MeOH$

atom	x	y	z	U_{eq}, Å^2
Mn(1)	−0.0380 (1)	0.1145 (1)	0.22396 (8)	0.0342 (5)
Na(1)	0.00000	0.00000	0.00000	0.044 (2)
Na(2)	0.00000	0.50000	0.50000	0.062 (2)
Na(3)	−0.2456 (3)	0.1778 (3)	0.6087 (2)	0.039 (1)
O(1)	−0.2407 (6)	0.0832 (5)	0.3054 (3)	0.044 (3)
O(2)	−0.1553 (5)	−0.0946 (5)	0.1546 (3)	0.040 (2)
O(3)	0.0539 (6)	0.3356 (6)	0.2993 (3)	0.045 (3)
O(4)	−0.0676 (5)	0.1918 (5)	0.1305 (3)	0.035 (2)
O(5)	0.0235 (6)	0.0610 (5)	0.3243 (4)	0.043 (3)
O(6)	0.1508 (5)	0.1193 (5)	0.1506 (3)	0.037 (2)
O(7)	−0.4971 (6)	−0.0978 (6)	0.3224 (5)	0.076 (3)
O(8)	0.1231 (7)	0.5805 (6)	0.2888 (4)	0.069 (3)
O(9)	0.2088 (6)	0.0077 (6)	0.3510 (4)	0.060 (3)
O(10)	0.0236 (6)	0.2695 (6)	0.5133 (4)	0.055 (3)
O(11)	−0.2720 (6)	0.2875 (6)	0.4803 (4)	0.052 (3)
C(1)	−0.3628 (9)	−0.0579 (9)	0.2772 (6)	0.047 (4)
C(2)	−0.3234 (8)	−0.1660 (8)	0.1825 (5)	0.042 (4)
C(3)	−0.376 (1)	−0.3297 (9)	0.2042 (7)	0.065 (5)
C(5)	−0.412 (1)	−0.186 (1)	0.0986 (6)	0.065 (5)
C(5)	0.0637 (9)	0.4354 (9)	0.2514 (6)	0.044 (4)
C(6)	0.0001 (8)	0.3622 (7)	0.1499 (5)	0.035 (3)
C(7)	−0.135 (1)	0.4034 (9)	0.1493 (6)	0.058 (5)
C(8)	0.141 (1)	0.4216 (9)	0.0689 (6)	0.057 (4)
C(9)	0.1549 (9)	0.0423 (8)	0.2972 (5)	0.042 (4)
C(10)	0.2337 (8)	0.0687 (8)	0.1929 (5)	0.043 (4)
C(11)	0.408 (1)	0.193 (1)	0.1984 (8)	0.078 (6)
C(12)	0.217 (1)	−0.097 (1)	0.1242 (6)	0.079 (6)
C(13)	0.144 (1)	0.284 (1)	0.5652 (7)	0.070 (5)
C(14)	−0.417 (1)	0.304 (1)	0.4932 (7)	0.075 (5)

$^a U_{eq} = (1/3)\sum_i\sum_j U_{ij} a_i^* a_j^* \bar{a}_i \cdot \bar{a}_j$.

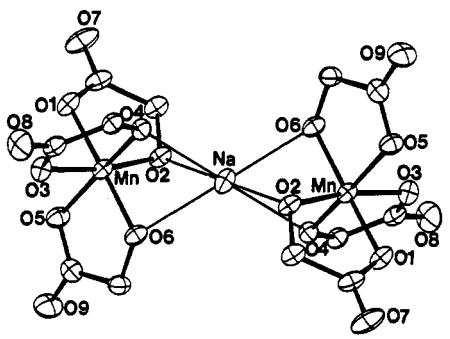

Figure 2. ORTEP diagram of the $[Na^{I}Mn^{IV}_2(HIB)_6]^{3-}$ "cluster" with Mn(IV)–O bonds in bold lines and Na–O bonds in thin lines. Methyl groups of the HIB ligand have been omitted for clarity.

from a least-squares refinement of 15 reflection settings obtained from an automatic centering routine. Table II contains a summary of data collection conditions for **1** and **5**. The data were reduced by using the SHELX76 program package and the structure was solved by using SHELX86.[23] In the subsequent refinement, the function $\sum w(|F_o| - |F_c|)^2$ was minimized where $|F_o|$ and $|F_c|$ are the observed and calculated structure factor amplitudes. The agreement indices $R = \sum||F_o| - |F_c||/|F_o|$ and $R_w = [\sum w(|F_o| - |F_c|)^2/\sum w|F_o|^2]^{1/2}$ were used to evaluate the results. Atomic scattering factors are from ref 24. Hydrogen atoms were located, but not refined, and placed at fixed distances from bonded carbon atoms of 0.95 Å in the final least-squares refinement. All hydrogen atoms were given fixed U values (isotropic temperature factors) calculated as $U_H = 1.3U_C$ Å^2). Fractional atomic coordinates for all non-hydrogen atoms of **1** and **5** are given in Tables III and IV, respectively. Tables V and VI list selected bond distances and angles for these compounds. Figure 2 provides an ORTEP diagram of the mixed-metal cluster $Na[Mn(HIB)_3]_2^{3-}$, and Figure 3 shows an ORTEP diagram that focuses on the Mn(IV) coordination sphere of a single $Mn(HIB)_3^{2-}$ unit. An ORTEP diagram of the $Mn^{III}_2(Lc)_4(HL)^{3-}$ ion is illustrated in Figure

Table IV. Fractional Atomic Coordinates for $(TMA)_3[Mn^{III}_2(Lc)_2HLc]\cdot H_2O$

atom	x	y	z	U_{eq},^{a} Å^2
Mn(1)	0.2815 (2)	0.18758	0.1117 (2)	0.0417 (8)
Mn(2)	0.1647 (2)	0.1650 (2)	0.3115 (2)	0.0438 (9)
O(1)	0.329 (1)	0.3164 (7)	0.0882 (9)	0.053 (4)
O(2)	0.485 (1)	0.3952 (8)	0.073 (1)	0.082 (6)
O(3)	0.435 (1)	0.1656 (7)	0.0939 (9)	0.064 (4)
O(4)	0.1767 (9)	0.1793 (8)	−0.0572 (8)	0.057 (4)
O(5)	−0.017 (1)	0.173 (1)	−0.1610 (9)	0.085 (5)
O(6)	0.1281 (8)	0.2092 (6)	0.1348 (8)	0.041 (4)
O(7)	0.142 (1)	0.2845 (8)	0.3706 (9)	0.057 (5)
O(8)	−0.001 (1)	0.3690 (8)	0.407 (1)	0.077 (6)
O(9)	0.010 (1)	0.1460 (7)	0.325 (1)	0.062 (5)
O(10)	0.281 (1)	0.1252 (9)	0.4721 (9)	0.066 (5)
O(11)	0.475 (1)	0.099 (1)	0.562 (1)	0.119 (7)
O(12)	0.3206 (8)	0.1906 (7)	0.2903 (8)	0.046 (4)
O(13)	0.269 (1)	0.0485 (8)	0.126 (1)	0.070 (5)
O(14)	0.164 (1)	0.0375 (8)	0.258 (1)	0.072 (6)
O(15)	0.320 (2)	−0.119 (1)	0.140 (2)	0.16 (1)
C(1)	0.438 (2)	0.321 (1)	0.083 (1)	0.048 (6)
C(2)	0.507 (2)	0.238 (1)	0.087 (2)	0.067 (8)
C(3)	0.556 (2)	0.227 (2)	−0.013 (2)	0.11 (1)
C(4)	0.062 (1)	0.180 (1)	−0.068 (1)	0.052 (6)
C(5)	0.027 (1)	0.190 (1)	0.042 (1)	0.059 (6)
C(6)	−0.073 (2)	0.261 (2)	0.026 (2)	0.10 (1)
C(7)	0.035 (2)	0.297 (1)	0.381 (1)	0.053 (7)
C(8)	−0.053 (2)	0.219 (1)	0.353 (2)	0.059 (7)
C(9)	−0.105 (2)	0.199 (1)	0.449 (2)	0.084 (9)
C(10)	0.390 (2)	0.123 (1)	0.482 (2)	0.068 (8)
C(11)	0.428 (1)	0.160 (1)	0.374 (1)	0.055 (6)
C(12)	0.521 (2)	0.230 (1)	0.404 (2)	0.089 (9)
C(13)	0.229 (2)	0.005 (1)	0.200 (2)	0.066 (8)
C(14)	0.256 (2)	−0.089 (1)	0.213 (2)	0.09 (1)
C(15)	0.336 (4)	−0.106 (2)	0.337 (3)	0.27 (3)
O(16)	0.534 (1)	0.998 (1)	0.122 (1)	0.116 (8)
N(1)	0.850 (1)	0.904 (1)	0.259 (1)	0.076 (7)
C(16)	0.836 (3)	0.937 (2)	0.142 (2)	0.14 (2)
C(17)	0.980 (2)	0.875 (2)	0.310 (2)	0.12 (1)
C(18)	0.765 (3)	0.832 (2)	0.260 (3)	0.15 (2)
C(19)	0.827 (3)	0.975 (1)	0.330 (2)	0.12 (1)
N(2)	0.253 (1)	0.4992 (8)	0.267 (1)	0.045 (5)
C(20)	0.306 (2)	0.560 (1)	0.201 (2)	0.079 (8)
C(21)	0.341 (2)	0.432 (1)	0.325 (1)	0.067 (7)
C(22)	0.144 (1)	0.455 (1)	0.186 (2)	0.071 (7)
C(23)	0.214 (2)	0.551 (1)	0.354 (1)	0.078 (8)
N(3)	0.751 (1)	0.5119 (9)	0.258 (1)	0.054 (6)
C(24)	0.858 (1)	0.563 (1)	0.332 (1)	0.070 (8)
C(25)	0.710 (2)	0.447 (1)	0.333 (1)	0.062 (7)
C(26)	0.648 (1)	0.573 (1)	0.203 (2)	0.067 (8)
C(27)	0.785 (2)	0.461 (1)	0.166 (1)	0.070 (8)

$^a U_{eq} = (1/3)\sum_i\sum_j U_{ij} a_i^* a_j^* \bar{a}_i \cdot \bar{a}_j$.

Table V. Selected Bond Lengths (Å) and Angles (deg) for $Na_3[NaMn^{IV}_2(HIB)_6]\cdot 4MeOH$

Mn(1)–O(1)	1.931 (4)	Mn(1)–O(2)	1.849 (4)
Mn(1)–O(3)	1.933 (4)	Mn(1)–O(4)	1.835 (4)
Mn(1)–O(5)	1.932 (5)	Mn(1)–O(6)	1.839 (4)
Mn(1)–Na(1)	2.977 (1)	Na(1)–O(2)	2.472 (4)
Na(1)–O(4)	2.412 (3)	Na(1)–O(6)	2.467 (4)
O(1)–Mn(1)–O(2)	84.6 (2)	O(1)–Mn(1)–O(3)	88.0 (2)
O(1)–Mn(1)–O(4)	95.9 (2)	O(1)–Mn(1)–O(5)	89.3 (2)
O(1)–Mn(1)–O(6)	172.1 (1)	O(2)–Mn(1)–O(3)	171.1 (2)
O(2)–Mn(1)–O(4)	90.9 (2)	O(2)–Mn(1)–O(5)	96.3 (2)
O(2)–Mn(1)–O(6)	90.8 (2)	O(3)–Mn(1)–O(4)	85.1 (2)
O(3)–Mn(1)–O(5)	88.5 (2)	O(3)–Mn(1)–O(6)	97.1 (2)
O(4)–Mn(1)–O(5)	171.6 (2)	O(4)–Mn(1)–O(6)	90.5 (2)
O(5)–Mn(1)–O(6)	84.9 (2)	Mn(1)–O(2)–Na(1)	85.8 (1)
Mn(1)–O(4)–Na(1)	87.9 (1)	Mn(1)–O(6)–Na(1)	86.2 (2)
O(2)–Na(1)–O(4)	65.0 (1)	O(2)–Na(1)–O(6)	64.2 (1)
O(4)–Na(1)–O(6)	64.6 (1)		

(23) Computations were carried out on an Amdahl 5860 computer. Computer programs used during the structural analysis were from the SHELX program package by George Sheldrick, Institut für Anorganische Chemie der Universität Göttingen, Göttingen, Federal Republic of Germany. Other programs used included ORTEP, a thermal ellipsoidal drawing program by C. K. Johnson, and the SHELXTL-PLUS program package.

(24) *The International Tables for X-Ray Crystallography*; Ibers, James A., Hamilton, Walter C., Eds.; Kynoch Press: Birmingham, England, 1974; Vol. IV, Table 2.2 and 2.3.1.

(25) Larson, E.; Lah, M. S.; Li, X.; Bonadies, J. A.; Pecoraro, V. L. Submitted for publication in *Inorg. Chem.*

Table VI. Selected Bond Lengths (Å) and Angles (deg) for $(TMA)_3[Mn^{III}_2(Lc)_2HLc]$

Mn(1)-O(1)	2.08 (1)	Mn(1)-O(3)	1.86 (1)
Mn(1)-O(4)	2.061 (9)	Mn(1)-O(6)	1.88 (1)
Mn(1)-O(12)	2.080 (9)	Mn(1)-O(13)	2.13 (1)
Mn(2)-O(6)	2.167 (9)	Mn(2)-O(7)	2.00 (1)
Mn(2)-O(9)	1.84 (1)	Mn(2)-O(10)	2.11 (1)
Mn(2)-O(12)	1.91 (1)	Mn(2)-O(14)	2.05 (1)
Mn(1)-Mn(2)	3.094 (4)		
O(1)-Mn(1)-O(3)	82.0 (5)	O(1)-Mn(1)-O(4)	93.4 (5)
O(1)-Mn(1)-O(6)	98.4 (4)	O(1)-Mn(1)-O(12)	97.7 (4)
O(1)-Mn(1)-O(13)	167.2 (5)	O(3)-Mn(1)-O(4)	100.1 (5)
O(3)-Mn(1)-O(6)	178.2 (4)	O(3)-Mn(1)-O(12)	100.1 (4)
O(3)-Mn(1)-O(13)	85.3 (5)	O(4)-Mn(1)-O(6)	81.6 (4)
O(4)-Mn(1)-O(12)	157.9 (4)	O(4)-Mn(1)-O(13)	89.2 (5)
O(6)-Mn(1)-O(12)	77.1 (4)	O(6)-Mn(1)-O(13)	94.4 (5)
O(12)-Mn(1)-O(13)	86.4 (4)		
O(6)-Mn(2)-O(7)	93.6 (4)	O(6)-Mn(2)-O(9)	102.2 (4)
O(6)-Mn(2)-O(10)	153.4 (5)	O(6)-Mn(2)-O(12)	74.4 (4)
O(6)-Mn(2)-O(14)	89.9 (5)	O(7)-Mn(2)-O(9)	83.4 (5)
O(7)-Mn(2)-O(10)	92.5 (5)	O(7)-Mn(2)-O(12)	94.9 (5)
O(7)-Mn(2)-O(14)	171.2 (5)	O(9)-Mn(2)-O(10)	104.1 (5)
O(9)-Mn(2)-O(12)	176.2 (4)	O(9)-Mn(2)-O(14)	87.9 (5)
O(10)-Mn(2)-O(12)	79.4 (5)	O(10)-Mn(2)-O(14)	88.0 (5)
O(12)-Mn(2)-O(14)	93.9 (5)		
Mn(1)-O(6)-Mn(2)	99.5 (4)	Mn(1)-O(12)-Mn(2)	101.6 (3)

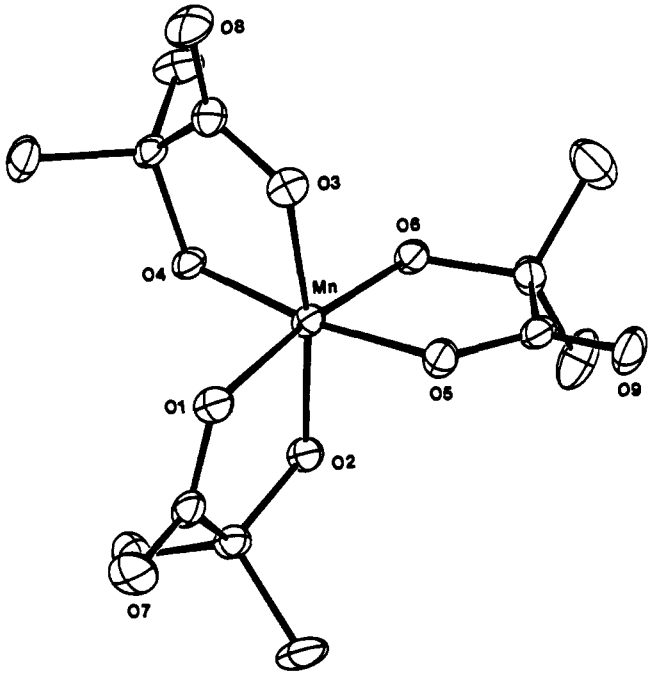

Figure 3. ORTEP diagram of one of the $[Mn^{IV}(HIB)_3]^{2-}$ octahedra as viewed down the apparent 3-fold axis defined by the coordinated alkoxide oxygen atoms.

4. Unique data and final R indices for both structures are reported in Table II.

Orthorhombic crystals of **6** with unit cell parameters a = 15.102 (6), b = 20.083 (12), and c = 19.394 (9) Å were consistently of poor quality and the structure could not be solved reliably. There was significant disorder in the alkylammonium cations, although the $Mn^{III}(HEB)_2$ unit was well behaved and appeared to form a tetragonal plane for a repeating chain structure. Repeated attempts to generate crystals from different solvents, with different cations, and with the lactic acid derivative were unsuccessful. Because of the poor quality of this structure, we have refrained from describing it in detail; however, the basic chain motif that is illustrated in Figure 5 is completely consistent with redox titration, elemental analyses, density (MW 929 g/mol), spectroscopic studies, and previous structural precedents.

Results and Discussion

Generation of Complexes. The Mn(IV) complexes described herein have been prepared via either an oxidative or a reductive methodology (defined by whether Mn is oxidized or reduced). The

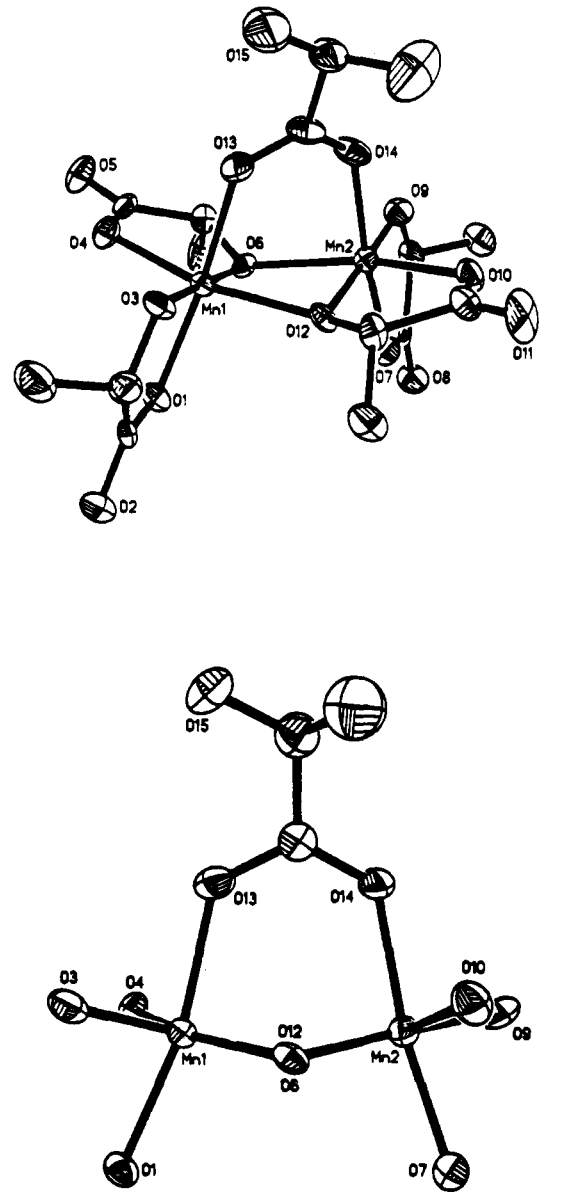

Figure 4. Top: ORTEP diagram of $[Mn^{III}_2Lc_4HLc]^{3-}$. Bottom: View of the manganese coordination sphere of $[Mn^{III}_2Lc_4HLc]^{3-}$ illustrating the deviation of the core from planarity.

oxidative procedure uses $MnCl_2$, Mn(acetate)$_2$, or manganese(III) acetate. In all cases, dioxygen is the oxidant following the stoichiometry of eq 4. The reductive method employs salts of

$$\text{Mn salt} + 3H_2L + 6\,\text{base} \rightarrow [Mn^{IV}L_3]^{2-} \quad (4)$$

permanganate (sodium, potassium, and TBA) and excess ligand, which acts as a sacrificial reductant of the MnO_4^- as illustrated in eq 5 releasing CO_2. The resultant ketone is dependent on the

$$(Cat)Mn^{VII}O_4 + 4.5H_2L + (Cat)OH \rightarrow (Cat)_2[Mn^{IV}L_3] + 1.5\,\text{ketone} + 1.5CO_2 + 5H_2O \quad (5)$$

starting ligand (e.g., HIB gives acetone). Both methods led to high product yields; however, we prefer the reductive procedure when forming $(Cat)_2[Mn^{IV}(HIB)_3]$ (eq 5) since it is faster and can more easily substitute cations and the yield is less sensitive to the rate of addition of reactants. It should be stressed, however, that the prefered preparation of $(Cat)_2[Mn^{IV}Lc_3]$ is via the oxidative route. This is because the lactic acid is much more sensitive to oxidation by permanganate than HIB and the resulting acetaldehyde can be further oxidized by permanganate to give acetate. Under these conditions, the red color of the $[Mn^{IV}Lc_3]^{2-}$ is initially obtained but this anion rapidly converts to a pale brown material of composition $\{(Cat)_2[Mn^{III}Lc_2(OAc)]\}_n$.

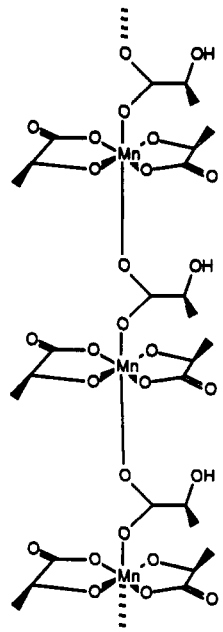

Figure 5. Proposed structure of $[Mn^{III}Lc_2HLc]^{2-}$. The infinite chain is consistent with a preliminary X-ray analysis, redox titration, magnetic susceptibility, elemental analysis, and density measurements. The acetate-bridged chain structure also is a well-defined structural motif for Mn(III) materials and is likely for materials of composition $[Mn^{III}Lc_2(acetate)]^{2-}$

In addition to the X-ray structure described below, the oxidation state and chemical composition of these materials were confirmed by redox titration, which yields 2 electrons per manganese, elemental analysis, solid-state and solution magnetic susceptibility measurements (≈4.0 μ_B/Mn), and EPR spectroscopy (vide infra). Neither the $[Mn(HIB)_3]^{2-}$ ion nor the $[Mn(Lc)_3]^{2-}$ ion exhibits metal-centered electrochemistry in methanol, DMF, or acetonitrile over a potential window of 2 V (+1 to −1 V vs SCE). This is not surprising since we have shown previously that coordinated alkoxides strongly stabilize higher manganese oxidation states. In neutral compounds where two alkoxides are bound to an Mn(IV) [e.g., $Mn(SALADHP)_2$] the quasi-reversible one-electron reduction occurred at ≈−350 mV vs SCE. A combination of an added third alkoxide and a total dinegative charge on the $[Mn(HIB)_3]^{2-}$ ion leads to even lower accessibility of the Mn(III) oxidation level.

Although the MnL_3 stoichiometry does not support manganese(III) α-hydroxy acid compounds, stable species can be isolated with Mn(III):L ratios of 1:2.5. Either the reductive or oxidative syntheses can be employed; however, once again the reductive procedures (eq 6 and 7) lead to higher yields and purer materials.

$$2(Cat)Mn^{VII}O_4 + 7H_2Lc + (Cat)OH \rightarrow (Cat)_3[Mn^{III}_2Lc_4(HLc)] + 2HOAc + 2CO_2 + 7H_2O \quad (6)$$

$$(Cat)Mn^{VII}O_4 + 5H_2HEB + (Cat)OH \rightarrow (Cat)_2[Mn^{III}HEB_2(HHEB)] + 2\,\text{pentanone} + 2CO_2 + 5H_2O \quad (7)$$

The chemical composition, metal oxidation states, and structural motifs are demonstrated by redox titration of the complexes, which yield 1 electron per manganese, elemental analysis, magnetic susceptibility measurements [a weakly coupled antiferromagnet with μ = 4.71 μ_B/Mn in the solid, which increases to single ion magnetism in solution 4.94 μ_B/Mn] and X-ray analysis [although the structure of $(TBA)_2[Mn^{III}HEB_2(HHEB)]$ is of marginal quality]. Unlike **1**–**3** or Mn(II) materials, these compounds are EPR silent at X-band frequencies when standard detection geometrics are used.

Structural Description of 1, 5, and 6. Figures 2 and 3 provide ORTEP diagrams of the mixed-metal, trinuclear core of the $Na_2[Mn(HIB)_3]\cdot 2CH_3OH$ structure and a view down the pseudo 3-fold axis generated by the facial alkoxide coordination to one of the manganese atoms of the cluster, respectively. The Mn(IV) ions are six-coordinate with a facial orientation of alkoxide and carboxylate ligands. The $Mn-O_{alk}$ distances (average = 1.841 ± 0.006 Å) are significantly shorter than the $Mn-O_{carb}$ distances (average = 1.932 ± 0.004 Å), which results in a trigonal distortion of the Mn(IV) polyhedron. Cooper[13] observed a similar phenomenon in the $Mn(DTBC)_3^{2-}$ anion and explained the structure in terms of the short catechol bite distance. A regular octahedral structure with a 1.91 Å Mn–O distance requires a 2.7-Å bite distance. Ligands with significantly shorter bite distances and angles such as the catecholates (2.58 Å; 85°) or HIB (2.54 Å; 85°) impart a trigonal compression on the Mn(IV) coordination sphere. The distances and angles observed for $[Mn(HIB)_3]^{2-}$ are very similar to those of $Mn(DTBC)_3^{2-}$. This observation provides further support for the Cooper formulation of $Mn(DTBC)_3^{2-}$ as a manganese(IV) tris(catecholate) rather than a manganese(III) bis(catecholate) semiquinone since $[Mn(HIB)_3]^{2-}$ contains entirely redox-innocent ligands.

Another interesting structural feature of the red crystals is the bridging sodium atom, illustrated in Figure 2, which is located on a crystallographic inversion center. The Mn(IV) polyhedra are linked through the trigonal faces containing alkoxide oxygens and this sodium ion. The Mn(IV)–Na(I) separation is 2.977 (1) Å, a distance that is much shorter than many Mn–Mn separations in discrete manganese clusters. Thus, one might consider the basic structural unit of the crystal as a $[Na^{I}Mn^{IV}_2(HIB)_6]^{3-}$ cluster rather than solely as discrete Mn(IV) distorted octahedra. We have recently reported[1d] another mixed manganese/sodium cluster, $\{Na^{I}[Mn^{III}(2\text{-OH-SALPN})(OAc)_2]_2\}^{+}$ (**8**) with an Mn–Na separation of 3.27 Å. The 0.3-Å elongation in **8** is more a consequence of the differences in polyhedral sharing (**1** is face shared while **8** is edge shared) than oxidation state or bridging heteroatom distances.

In addition to the formation of a lactic acid complex which is isostructural with **1**, a Mn(III) dimer (**5**) can be isolated as illustrated in Figure 4. Each Mn(III) ion has two bidentate, dianionic lactates (*S* configuration) bound in a cis propeller configuration. Dimerization of these units is achieved by bridging alkoxides from one of the two bound lactates (O(6) and O(12)) on each of the Mn(III) and by a fifth lactate, a monoanion with protonated hydroxyl oxygen O(15), that forms a syn carboxylate bridge by using O(13) and O(14). A unique aspect of this dimer is the axial compression of the Mn(III) octahedra. In general, high-spin d^4 ions undergo a Jahn–Teller distortion to relieve the degeneracy of the e_g electron. With rare exceptions, Mn(III) adopts an axial elongation; however, the generally weak ligand set in **5** leads to four long bonds from a bridging alkoxide and three carboxylate oxygens (for the Mn(1) octahedron (Å): Mn(1)–O(1), 2.08 (1); Mn(1)–O(4), 2.061 (9); Mn(1)–O(12), 2.080 (9); Mn(1)–O(13), 2.13 (1) and two short bonds of coordinated alkoxides (Mn(1)–O(3), 1.86 (1) Å; Mn(1)–O(6), 1.88 (1) Å). This structural motif should lead to a rearrangement of the d-orbital energy levels, leaving d_{z^2} as the nonmagnetic orbital. We will report separately the effect of this distortion on the magnetic exchange in this and related systems.

A comparison of **5**, $[Mn^{III}(SALAHP)(OAc)]_2$ (**9**),[5c] and $[Mn^{III}(SALAHP)(Cl)(CH_3OH)]_2$ (**10**) illustrates the flexibility associated with dialkoxide-bridged structures. The latter two complexes have planar $(Mn-OR)_2$ cores with bridging acetates and unidentate chloride and methanol ligands, respectively, while Figure 4 illustrates how the bridging lactate causes the Mn(1)–O(6)–Mn(2)–O(12) core of **5** to deviate from planarity. In contrast to **5**, both **9** and **10** exhibit axial Jahn–Teller elongations that are perpendicular to the $(Mn-OR)_2$ plane. Therefore, **9** (2.87 Å) and **10** (3.01 Å) show short Mn–Mn separations relative to **5** (3.094 (4) Å). It is apparent that one can observe a wide range of Mn(III)–Mn(III) separations by using the dialkoxide bridge motif.

Although we can not directly determine the Mn(IV)–Mn(IV) separation in a trialkoxide-bridged structure using **1** due to the intervening Na atom, we can make a reasonable estimate for this distance by "fusing" the two Mn polyhedra in a hypothetical

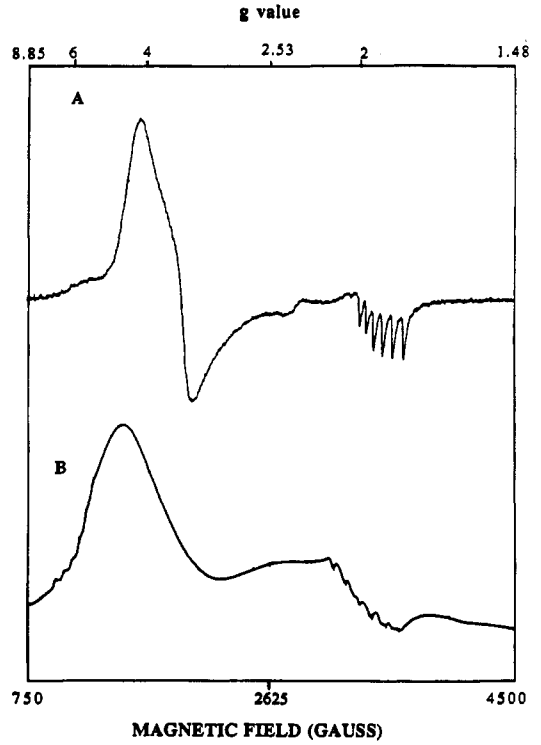

Figure 6. X-Band (0.3 GHz) EPR spectra of (A) **1** and (B) **4** in DMF at 100 K. The spectrum of complex **4** shows two overlapping sets of lines from **4** and a small amount of Mn(II) impurity in the $g = 2$ region.

face-shared geometry. Our estimate using the bond distances and angles in Tables V is 2.42 Å. This might appear unrealistic at first glance; however, Wieghardt has reported[4c] an $Mn^{IV}_2(\mu_2\text{-}O)_3$ core with an incredible 2.296-Å metal separation. In this light, our estimate for the $Mn^{IV}_2(\mu_2\text{-}OR)_3$ core is reasonable.

We will refrain from any quantitative structural description of **6** because of the poor data quality obtained on three independent crystals. An infinite chain in which $[Mn^{III}HEB_2]^-$ planes are linked through the oxygens of a bridging anti–anti carboxylate of $HHEB^-$ illustrated as Figure 5 is our best model for the structure. This formulation is consistent with all analytical data and has previous structural precedent in the structures of Mn^{III}(SALEN)(OAc),[26] Mn^{III}(2-OH-SALPN)(OAc)[1d] and $\{(NH_4)_2[Mn^{III}(SAL)_2(CH_3OH)_2][Mn^{III}(SAL)_2]\}_n$.[27] Unlike the propeller structure in **5** the HEB ligands are oriented in a planar configuration. Although **6** has a metal:ligand stoichiometry identical with that of **1**, we have been unable to isolate the corresponding $[Mn^{IV}(HEB)_3]^{2-}$ material. This may be due to the steric demands on placing multiple ethyl groups in the close proximity of the shared octahedral faces. Apparently, **6** is stable as the Mn(III) complex because the third alkoxide is protonated and uncoordinated.

Physical Properties of the Materials. The X-band EPR spectra of **1** and **4** in DMF are illustrated in Figure 6 and the spectral parameters reported in table 1. The trigonally distorted **1** shows a derivative-like spectrum ($g_{eff} = 3.9$ (crossover point)) with only traces of the ^{55}Mn nuclear hyperfine coupling on the component at $g = 2$. The Mn(IV) ion is a d^3 system and can be treated theoretically by using the literature developed for Cr^{3+} compounds,[28] spin quartet iron sulfur centers,[29] and previous Mn(IV) compounds.[1,30] The X-band spectrum of a d^3 ion is dependent on whether the electronic symmetry is axial or rhombic. Examples of the latter case[1h] (e.g., Mn^{IV}(SALADHP)$_2$) have absorptive features and g_{eff} ranges from 4 to 6 with larger g_{eff} values as the rhombicity increases. In an axial field ($E/D = 0$), the spectrum is dependent on the magnitude of the zero-field splitting parameters. Two limiting cases are defined when the value of the axial field (2D) is either much larger than or much smaller than $h\nu$ (0.31 cm^{-1}). The $g_{eff} = 2$ feature should dominate when D is very small. This is observed for tris(thiohydroxamato)manganate(IV)[30a] and tris(thiocarbamato)manganate(IV).[30b] When D is large, the $g_{eff} = 2$ feature should diminish and the dominant signal will appear at low field ($g_{eff} \approx 4$). This is observed for tris(catecholato)manganate(IV),[30c] tris(sorbilato)manganate(IV),[30d] and $Mn^{IV}(SALAHP)_2$.[1h] Because of the similarity in structure to tris(catecholato)manganate(IV), it is not surprising that **1** and **4** have EPR spectra that are of the latter variety (stong $g_{eff} \approx 4.25$ with a weaker component at $g_{eff} \approx 2$). A faint signal ($g_{eff} \approx 5.9$, with ^{55}Mn hyperfine coupling (71 G)) arises from a small thermal population of the first excited doublet. A value of $E/D \approx 0.05$ is consistent with these g_{eff} values. One expects the signal to appear less absorptive and more derivative-like as E/D approached zero. This trend is consistent in comparing the spectrum of **1** or **2** with that of $Mn^{IV}(SALADHP)_2$. The low-field features of the Mn(IV) complexes tend to be broad (≈450 G) and the appearance of ^{55}Mn hyperfine coupling tends to be variable. The Mn(III) complexes are EPR silent when a parallel detection mode is used.

The visible spectra of the Mn(IV) and Mn(III) complexes are featureless. In general, the complexes are red to brown due to a strong UV absorbance that tails into the visible. Only **5** shows a resolved visible absorption peak [410 nm ($\epsilon = 710$)]. Complex **6** displays visible absorption shoulders [405 ($\epsilon = 296$) and 515 nm ($\epsilon = 140$)] on an intense UV transition. The Mn(IV) complex **1** has a broad, unresolved band at ≈550 nm ($\epsilon = 296$). The α-hydroxy acids show reductive electrochemistry with waves centered between −900 and −1200 mV vs SCE. In contrast, the manganese complexes exhibit completely irreversible oxidative electrochemistry, centered at ≈1000 mV vs SCE (acetonitrile); however, we cannot establish whether this oxidation is metal or ligand centered.

Relationship to Biological Systems. Monomer/Trimer Model for the OEC. Considerable controversy surrounds the assignment of cluster nuclearity in the oxygen-evolving complex. The two main classes are either single center or dual center.[6] The former include tetranuclear cubanes or butterfly clusters.[2,6,7] The dual center models have either two sets of dimers,[10] two monomers and a dimer,[11] or a monomer and a trimer.[1,9] A feature of the last two proposals is that the low-field EPR signal of the S_2 state is associated with an isolated Mn(IV) center rather than a higher aggregate cluster.[11,31]

We have systematically prepared mononuclear Mn(IV) complexes in a variety of ligation states to evaluate the hypothesis of Hansson et al.[11] that the low-field signal arises from such a mononuclear center. Criticisms of this model have included the proposition that low-field signals of monomeric Mn(IV) will show ^{55}Mn hyperfine coupling, that the signals should be absorptive rather than derivative shaped, and that they will not give g_{eff} values at $g \approx 4.1$. In this vein, the EPR spectra of **1** and **2** can be compared with the observations of the photosynthetic system. First, these mononuclear Mn(IV) complexes exhibit spectra in the $g = 4$–6 range, although they are still slightly more rhombic ($g_{eff} \approx 4.25$) than the biological signal. The features are derivative

(26) Kennedy, B. J.; Murray, K. S. *Inorg. Chem.* **1985**, *24*, 1552.
(27) Kirk, M. L.; Lah, M. S.; Raptopoulou, C.; Kessissoglou, D. P.; Hatfield, W.; Pecoraro, V. L. Submitted for publication in *Inorg. Chem.*
(28) Pederson, E.; Toflund, H. *Inorg. Chem.* **1974**, *13*, 1603. Hemper, J. C.; Morgan, L. O.; Lewis, W. B. *Inorg. Chem.* **1970**, *9*, 2064. Singer, L. S. *J. Chem. Phys.* **1955**, *23*, 379.
(29) Huynh, B. H.; Kent, T. A. *Advances in Mössbauer Spectroscopy*; Thosar, B. V., Iyengar, P. K., Srivasta, J. K., Bhargava, S. C., Eds.; Elsevier: New York, 1983; p 490.
(30) (a) Pal, S.; Ghosh, P.; Chakravorty, A. *Inorg. Chem.* **1985**, *24*, 3704. (b) Brown, K. L.; Golding, R. M.; Healy, P. C.; Jessop, K. J.; Ten, W. C. *Aust. J. Chem.* **1974**, *27*, 2075. (c) Magers, K. D.; Smith, C. G.; Sawyer, D. T. *Inorg. Chem.* **1980**, *19*, 492. (d) Richens, D. T.; Sawyer, D. T. *J. Am. Chem. Soc.* **1979**, *101*, 3681. (e) Rasmussen, P.; Been, K. M.; Hornyak, E. J. *J. Chem. Phys.* **1969**, *50*, 3647.
(31) We have been given a preprint of a paper which shows that the $g = 4.1$ signal has at least 16 lines (assigned to Mn nuclear hyperfine structure) when oriented samples of the OEC have been treated with ammonia. This suggests that, at least in these ammonia-treated samples, the $g = 4.1$ signal comes from a cluster: Kim, D. H.; Britt, R. D.; Klein, M. P.; Saver, K. *J. Am. Chem. Soc.*, in press.

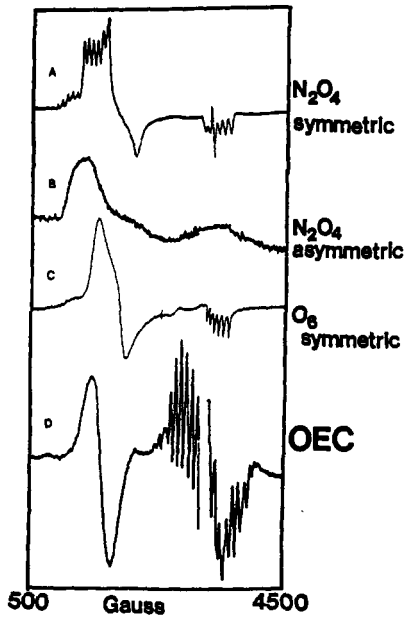

Figure 7. X-Band (9.3 GHz) EPR spectra (top to bottom) of (A) Mn(SALAHP)$_2$, (B) Mn(SALAHP)$_2$, (C) Mn(HIB)$_2^{2-}$, and (D) the S_2 state of the OEC. Spectra A–C were collected at 100 K and spectrum D was collected at ≈8 K. The 4 K spectra of **1** are essentially identical with spectrum C. Spectra A and B are modified from ref 1h. Spectrum D is modified from ref 7b.

shaped but do exhibit an asymmetry that is not observed in the biological sample. Both complexes are devoid of ^{55}Mn nuclear hyperfine coupling in the low-field region. One would expect that the $g_{eff} \approx 2$ hyperfine coupling would be obscured by the residual multiline signal in sample preparations. In general, the low-field features of the models tend to be broader (≈400 G) than the biological signal (250–300 G). To date, neither clusters nor monomers have adequately modeled all of the subtleties of the $g = 4$ signal; however, complex **1** is closer than other available models. A comparison of EPR spectra for three structurally characterized monomeric Mn(IV) complexes and the S_2 state of the OEC is shown in Figure 7.

Manganese Lignin Peroxidase. In certain fungi, manganese acts as a diffusible cofactor of a heme peroxidase that oxidatively degrades lignin.[20] Activity is stimulated by the presence of α-hydroxy acids such as lactic acid. The most likely catalytic cycle is oxidation of Mn(II) to Mn(III) by the heme, diffusion of the Mn(α-hydroxy acid) complex from the enzyme, and then radical oxidation of the polyphenolic substrate, causing polymer destruction. It is believed that the organic ligand is required to bias the metal redox potential to stabilize the Mn(III) oxidation state and possibly protect the manganese from disproportionating in aqueous solution back to Mn(II) and MnO_2.

Although it is now known that organic acids play a critical role in this process, chemically well-defined Mn(α-hydroxy acid) compounds have not been described previously. Our isolation of $(Cat)_3[(Cat)Mn^{IV}_2L_6]$, $(Cat)_3[Mn^{III}_2(L)_4HL]$ and $(Cat)_2[Mn^{III}(L)_2HL]$ demonstrates that α-hydroxy acids not only stabilize the Mn(III) oxidation level but also give isolable Mn(IV) complexes. We have shown that both bidentate (carboxylate/alkoxide) and monodentate (carboxylate) coordination is available through these ligands and that the higher oxidation level requires coordination of three alkoxide oxygens. It is unlikely that the $Mn^{IV}L_3^{2-}$ is a catalytic intermediate since it is very water sensitive and will decompose even in methanol in less than an hour. The Mn(III) complexes have higher aqueous stability; however, they will also decompose upon standing. While the lignin peroxidase uses hydrogen peroxide as a substrate, neither the Mn(III) nor Mn(IV) compounds will react with H_2O_2 or alkyl hydroperoxides; however, manganese(III) azide and thiocyanate complexes can be prepared directly from **5**. Armed with these well-characterized monomeric and dimeric materials, we are now in a position to evaluate the mechanism of manganese(III) α-hydroxy acid oxidation of phenols and, ultimately, lignin.

Acknowledgment. We express our gratitude to Profs. James Penner-Hahn and Michael Gold for valuable discussions on this topic and R. D. Britt and M. P. Klein for supplying us with a preprint of ref 31 prior to publication. We are grateful to the National Institutes of Health (Grant GM-39406) for support of this research. V.L.P. thanks the Alfred P. Sloan Foundation for a Fellowship (1989–91).

Supplementary Material Available: Tables 7 and 12, providing anisotropic thermal parameters for all non-hydrogen atoms, Tables 8 and 13, giving fractional atomic positions for hydrogen atoms, Tables 9 and 14, giving a complete set of bond distances, Tables 10 and 15, giving a complete set of bond angles for **1** and **5**, respectively, and Figures 8 and 9, providing complete numbering schemes for all atoms of **1** and **5** (16 pages); Tables 11 and 16, listing observed and calculated structure factors for **1** and **5**, respectively (19 pages). Ordering information is given on any current masthead page.